NANOSYSTEMS:
PHYSICS, CHEMISTRY, MATHEMATICS

Trukhanova K.A., et al. *Nanosystems: Phys. Chem. Math.*, 2025, **16** (1), 58–66.
http://nanojournal.ifmo.ru
DOI 10.17586/2220-8054-2025-16-1-58-66

Original article

Nanostructured transparent Fe^{2+}-doped lithium aluminosilicate glass-ceramics with tunable optical properties: effect of heat-treatment regimes on near-infrared absorption

Kristina A. Trukhanova[1,a], Olga S. Dymshits[2,3,b], Irina P. Alekseeva[3,c], Kirill V. Bogdanov[4,d], Svetlana S. Zapalova[3,e], Maksim I. Tenevich[2,f], Anastasia K. Bachina[2,g], Vadim I. Popkov[2,h], Aleksandr A. Zhilin[5,i]

[1]Nordwestlab LLC, St. Petersburg, Russia

[2]Ioffe Institute, St. Petersburg, Russia

[3]Vavilov State Optical Institute, St. Petersburg, Russia

[4]ITMO University, St. Petersburg, Russia

[5]D. V. Efremov Institute of Electrophysical Apparatus, pos. Metallostroi, St. Petersburg, Russia

[a]kristina.truhanova@gmail.com, [b]vodym1959@gmail.com, [c]vgolub19@gmail.com, [d]kirw.bog@gmail.com, [e]zenii99@yandex.ru, [f]mtenevich@gmail.com, [g]a.k.bachina@yandex.ru, [h]vip-07@yandex.ru, [i]zhilin1311@yandex.ru

Corresponding author: O.S. Dymshits, vodym1959@gmail.com

PACS 78.67.Bf, 61.46.Hk, 42.70.Ce, 64.75.Jk, 81.10.Aj, 78.20.Ci

ABSTRACT This study explores optical tuning of nanostructured transparent lithium aluminosilicate glass-ceramics nucleated by titania and doped with Fe^{2+} ions. The glass was melted at 1620 °C and heat-treated between 660 °C and 800 °C, yielding nanocrystals of γ-Al_2O_3 (2 – 23 nm) and β-quartz solid solutions (8 – 40 nm). Fe^{2+} ions in octahedral coordination in the initial glass are responsible for absorption in the 1000 – 1400 nm range. Tetrahedrally coordinated Fe^{2+} ions in γ-Al_2O_3 are responsible for absorption at 1550 – 2300 nm. Crystallization of β-quartz solid solutions leads to decreasing the γ-Al_2O_3 fraction and corresponding decrease of absorption at 1550 – 2300 nm. Differential scanning calorimetry, scanning electron microscopy, X-ray diffraction, Raman and optical spectroscopy reveal the relationship between heat-treatment regimes, crystalline phase development, and optical performance, highlighting the potential of Fe^{2+}-doped LAS glass-ceramics for advanced photonic applications. The glass-ceramics exhibit customizable optical properties, promising for saturable absorbers in passive Q-switching lasers.

KEYWORDS Nanophase glass-ceramics, γ-Al_2O_3 nanocrystals, nanocrystals of β-quartz solid solution, Fe^{2+} ions

ACKNOWLEDGEMENTS This work was partly supported by the Russian Science Foundation (Grant 23-23-00446).

FOR CITATION Trukhanova K.A., Dymshits O.S., Alekseeva I.P., Bogdanov K.V., Zapalova S.S., Tenevich M.I., Bachina A.K., Popkov V.I., Zhilin A.A. Nanostructured transparent Fe^{2+}-doped lithium aluminosilicate glass-ceramics with tunable optical properties: effect of heat-treatment regimes on near-infrared absorption. *Nanosystems: Phys. Chem. Math.*, 2025, **16** (1), 58–66.

1. Introduction

Transparent nanophase lithium aluminosilicate (LAS) glass-ceramics based on nanocrystals of lithium aluminosilicates with the structure of β-quartz were invented by Stookey more than sixty years ago [1], and they still remains the most commercially successful ones due to a combination of transparency, near zero thermal expansion coefficient, high mechanical strength and durability [2–5]. The LAS system remains the subject of numerous studies [6–25]. On the one hand, complex devices and new research methods are emerging, allowing one to reconsider previously formulated approaches to the development of these materials, their structure and the regularities of their formation [6–14]. On the other hand, even small changes in the basic composition, as well as the nature and concentration of nucleating agents, and the introduction of modifying, coloring, and luminescent ions make it possible to develop new transparent, heat-resistant and durable materials that meet new needs [15–20, 22, 22–25]. Precise control of the phase composition of glass-ceramics of

the LAS system allowed us to develop transparent glass-ceramics based on spinel and β-quartz solid solutions (ss) and doped with Ni^{2+} and Co^{2+} ions intended for thermal shock resistant color filters and saturable absorbers of Er lasers [23]. The aim of the present study is the development of transparent spinel-based glass-ceramics with selective doping of ferrous ions into tetrahedral positions in the crystals with spinel structure ensuring broadband absorption in the spectral range of 2 μm, which is promising for saturable absorbers in the near IR spectral range.

2. Experimental

2.1. Preparation of glass and glass-ceramics

The reagent grade lithium carbonate, alumina, silica, titania, and ferrous oxide were thoroughly mixed to prepare the glass with the composition 12 Li_2O, 24 Al_2O_3, and 64 SiO_2 (mol%) [26] nucleated by 6 mol% TiO_2 and doped with 0.1 % FeO added on top of the main components. The batch to produce 400 g of glass was placed into a crucible made of quartz ceramics and melted in a laboratory electric furnace at a temperature of 1620 °C with stirring, cast onto a cold metal plate and annealed at 640 °C for 0.5 h. The pieces of transparent pale-yellow glass were heat-treated by single and two-stage schedules in the temperature range of 660 to 1200 °C for 6 h at each stage. The samples obtained by heat-treatments up to 1000 °C were transparent and brown-colored. The complex character of the color variation with heat-treatment temperature is in relation to precipitated crystalline phases and will be discussed elsewhere. The glass-ceramic obtained by heat-treatments at 1100 °C was translucent, and that obtained at 1200 °C was opaque, see Fig. 1.

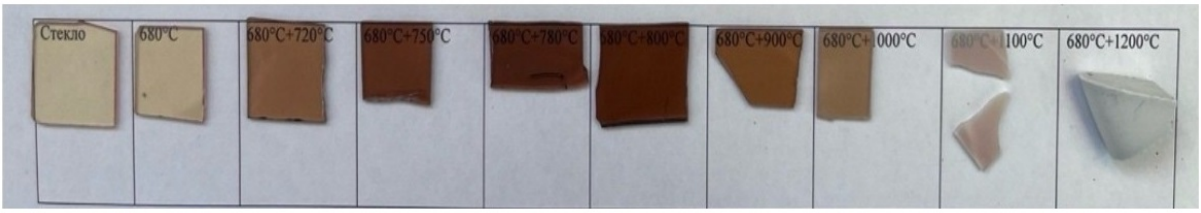

FIG. 1. Images of glasses and glass-ceramics. Transparent samples are polished plates with thickness of 1 mm.

2.2. Methods

Differential scanning calorimetry (DSC) of the initial as-quenched and heat-treated glasses with the weight of $\sim$ 15 mg was performed in a temperature range from 35 to 1300 °C in a flow of Ar using the simultaneous thermal analyzer NETZSCH STA 449 F3 Jupiter at a heating rate of 10 °C/min.

Raman spectra were recorded using a confocal InVia Renishaw Raman microscope equipped with a $\times$50 Leica objective (N.A. = 0.75), a TE cooled CCD camera and an edge filter. The spectra were excited by an Ar^+ ion laser line at 488 nm. The spectral resolution was 2 cm^{-1}. Every spectrum was averaged over 10 acquisitions with duration of 10 s.

The Tescan Vega 3 SBH scanning electron microscope was used to study the morphology of the materials. To obtain the scanning electron microscopy images, the surfaces of the samples were cleaned using isopropyl alcohol and benzene, then etched in a hydrofluoric acid for about 2 s and washed in distilled water. The particle size was estimated using ImageJ software [27].

The X-ray diffraction (XRD) experiments were performed on the Shimadzu XRD-6000 diffractometer operating with Cu Kα radiation and a Ni filter (λ = 1.5406 Å). The average crystal sizes were calculated from broadening of X-ray peaks according to Scherrer's equation [28]. The average size of γ-Al_2O_3 crystals was estimated from the peak with indices hkl (440); the size of tieilite crystals, Al_2TiO_5, from the peak with indices hkl (020). The average size of crystals of β-quartz ss was determined from the (220) peak, while the average size of crystals of β-spodumene ss was calculated using the (102) peak. The error in the estimation of the average crystal size is $\sim$ 5 – 10 %. The lattice parameter a of γ-Al_2O_3 nanocrystals was estimated from the position of the peak with Miller's indices hkl (440), those of Al_2TiO_5 from the peaks with indices (002), (020), (110), (023) and (200). The lattice parameters of β-quartz ss were estimated from the positions of the peaks with indices (110) and (211), while those of β-spodumene ss were estimated using the peaks with Miller's indices (111) and (102). The error is $\pm$0.003 Å.

Absorption spectra of polished flat-parallel plates with a thickness of $\sim$ 1 mm were measured using a Shimadzu UV-3600 spectrophotometer in the spectral range from 200 to 3300 nm.

Density was measured by the hydrostatic weighing in toluene at room temperature.

3. Results and discussion

The DSC traces of as-quenched and heat-treated glasses demonstrate a pronounced influence of preliminary heat-treatments on the character of phase transformations and the nature of crystalline phases, see Fig. 2. The DSC curve of the as-quenched glass is typical for glasses of the lithium aluminosilicate (LAS) system [29] nucleated by titanium

oxide. It shows the onset of the glass transition (T_g) at 698 °C. At higher temperatures, the DSC curve exhibits a strong exothermic peak with crystallization onset temperature $T_x = 852$ °C and crystallization peak temperature, $T_p = 873$ °C, which is explained by the crystallization of the lithium aluminosilicate with β-quartz structure [29]. Indeed, the XRD pattern of the as-quenched glass heated in the furnace of the DSC instrument up to 885 °C, which is the temperature at the end of the first exothermic peak, presents the lines of the β-quartz ss, the main crystalline phase characteristic of these glass-ceramics, see Fig. 3(a). There are also traces of tieilite, aluminum titanate, the crystalline phase of the nucleating agent [30]. Small peaks in the temperature range from ca. 950 to 1150 °C can be assigned to traces of minor phases and will not be discussed here. The second rather prominent peak also of low intensity is seen at $\sim$ 1177 °C, Fig. 2. This peak is usually attributed to the appearance of β-spodumene ss [29], the high-temperature crystalline phase characteristic of LAS glass-ceramics [1, 2]. The preliminary heat-treatment at 660 °C for 6 h predictably leads to a decrease in the crystallization peak temperature, T_p, by about 20 °C, see Fig. 2 and Table 1. The peak becomes broader and has a lower intensity at the maximum as compared with the exothermic peak of the as-quenched glass. The XRD pattern of this glass heated in the furnace of the thermal analyzer up to 900 °C, also demonstrates crystallization of β-quartz ss (not shown here). We observed the similar character of the gahnite crystallization peak behavior after preliminary heat-treatment in glasses of the zinc aluminosilicate system nucleated by titania [31]. The DSC curve of glass heat-treated at 680 °C for 6 h has quite a different shape. Instead of one sharp peak in the temperature range from 800 to 900 °C, it presents two peaks in the temperature range from ca. 800 to ca. 950 °C. The first peak with $T_p = 829$ °C is caused by crystallization of γ-Al_2O_3 with cubic spinel structure, see Fig. 3(b), while the second peak is assigned to β-quartz ss, see Fig. 3(a). An additional proof of the attribution of the first peak on the DSC curve of the sample preliminary heat-treated at 680 °C to spinel crystallization is the DSC trace of the sample, in which spinel has already crystallized. Fig. 3(b) shows the XRD pattern of the glass-ceramic obtained by the two-stage heat-treatment at 680 and 750 °C for 6 h at each stage, which demonstrates a distinct spinel peak at $2\theta = 66.7°$. The DSC thermograph of this sample is presented in Fig. 2. It shows all the DSC peaks with the exception of the low-temperature exothermal peak assigned to spinel crystallization. Thus, we unambiguously attribute the first prominent peak on the DSC curve of the sample preliminary heat-treated at 680 °C to spinel crystallization and the second intense peak to crystallization of β-quartz ss.

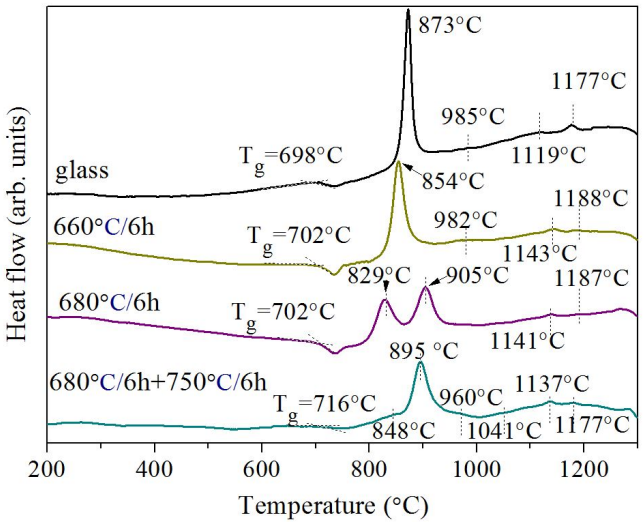

FIG. 2. DSC thermographs for the as-quenched and heat-treated glasses. The heat-treatment schedules are listed in figure. The curves are shifted for convenience of observation.

TABLE 1. Characteristic temperatures of the as-quenched and heat-treated glasses derived from DSC traces presented in Fig. 2.

Heat-treatment schedule, °C/h	T_g, °C	T_{p1}, °C	T_{p2}, °C
—	698±2	—	873±1
660/6	702±2	—	854±1
680/6	702±2	829±1	905±1
680/6+750/6	716±2	848±1	895±1

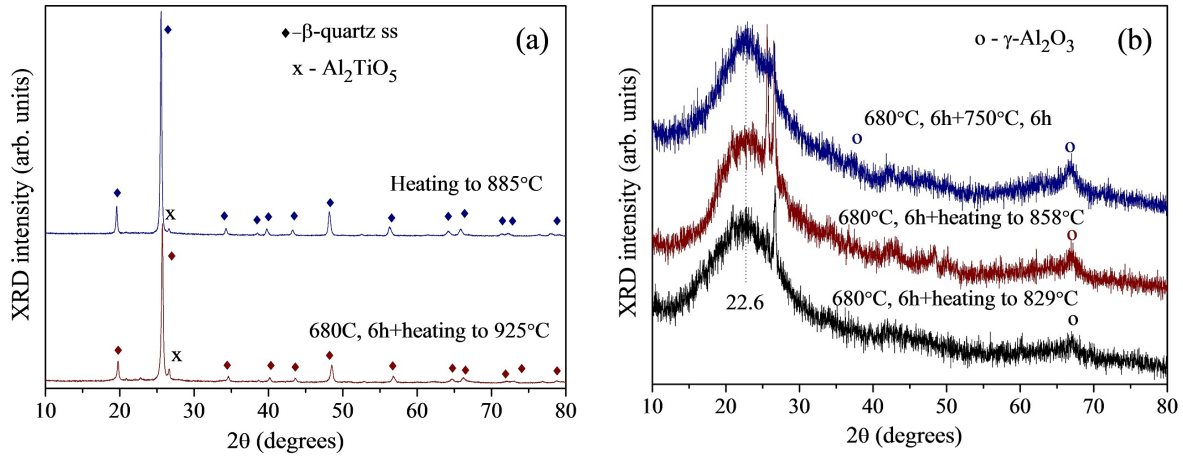

FIG. 3. XRD patterns of: (a) the as-quenched and heat-treated glasses heated in the furnace of the DSC instrument; (b) heat-treated glasses heated in the furnace of the DSC instrument and glass-ceramics obtained by the heat-treatment at 680 °C for 6 h and at 750 °C for 6 h added for comparison. The heat-treatment schedules are listed in figure. The curves are shifted for convenience of observation.

Taking into account the results of the DSC study, two-stage heat-treatments were conducted with the first stage at 680 °C for 6 h and the second stage in the temperature range of 720 to 800 °C for 6 h.

The Raman spectrum of the initial annealed glass shows a broad band with a maximum at 482 cm^{-1}, a band at 800 cm^{-1} and a broad band with maxima at ca. 917 cm^{-1} and ca. 1003 cm^{-1}, see Fig. 4. The wing of this band extends to 1200 cm^{-1}. The detailed arguments in favor of the attribution of the bands at 482 cm^{-1}, at 800 cm^{-1} and at 1003 cm^{-1} to the aluminosilicate glass network and the band located at ca. 917 cm^{-1} to titanium-oxygen tetrahedrons (TiO_4) built into this network can be found elsewhere [30]. Only minor changes are observed in the Raman spectrum of glass after its heat-treatment at 660 °C for 6 h. The peak in the range of wavenumbers from 850 to 1200 cm^{-1} becomes broader and has a flatter top, see Fig. 4.

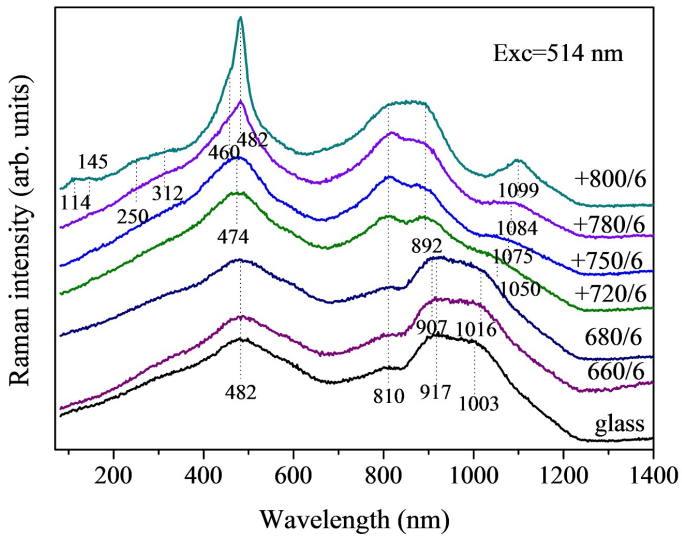

FIG. 4. Raman spectra of the initial and heat-treated glasses. $\lambda_{exc} = 514$ nm. The heat-treatment schedules (°C/h) are shown above the curves. The sign "+" designates the preliminary heat-treatment at 680 °C for 6 h. Numbers denote the position of the Raman peaks in cm^{-1}. The curves are shifted for the convenience of observation.

The maximum at 907 cm^{-1} becomes prominent in the Raman spectrum of the sample heat-treated at 680 °C for 6 h, and no other changes can be found in this spectrum as compared with the spectrum of the initial glass. The two-stage heat-treatment with the second stage at 720 °C results in significant modification of the Raman spectrum. The new band with two well-resolved maxima appears in the spectral range from 820 to 890 cm^{-1} and is assigned to (TiO_5) and (TiO_6) groups in aluminotitanate amorphous regions [30]. The high wavenumber wing of the broad band exhibits maximum at ca. 1050 cm^{-1}. The middle-range band becomes somewhat narrower, and its position slightly changes to 474 cm^{-1}.

These changes develop in spectra of the samples heat-treated at 750 and 780 °C at the second stage. The distinct feature of the Raman spectrum of the sample obtained by heat-treatment at 780 °C is a narrow band, which appears at 482 cm^{-1}. It is assigned to β-quartz ss [30]. In the Raman spectrum of the sample heat-treated at 800 °C at the second stage, there are bands with maxima at ca. 114, 482, and 1099 cm^{-1}, characteristic of solid solutions with β-quartz structure [32, 33]. A small peak at ca. 145 cm^{-1} is at the position of the strongest peak of metastable titania modification of anatase [32]. Two distinct maxima at 250 and 312 cm^{-1} are seen in a weak broad band located in the low wavenumber spectral range. Together with a strong and broad band with a maximum at ca. 890 cm^{-1}, they manifest crystallization of tieilite, Al_2TiO_5 [30].

The SEM images of all these samples demonstrate their inhomogeneous structure. This structure develops with an increase in the heat-treatment temperature, see Fig. 5. Fig. 5(a) shows that the annealed glass has a bimodal structure with smaller particle sizes of 5 – 10 nm and larger particle sizes of ca. 15 – 30 nm. The average particle size is 14 nm. The morphology of the glass heat-treated at 680 °C for 6 h demonstrates a broader particle size distribution with a somewhat smaller average particle size of 12 nm, see Fig. 5(b). The morphology of the sample obtained by a two-stage heat-treatment with a temperature of 720 °C at the second stage is composed of large particles with sizes ranging from 15 nm to ca. 60 nm and an average size of 31 nm, see Fig. 5(c). After heat-treatments at 750 °C, see Fig. 5(d), the particle sizes are similar to those in materials obtained by heat-treatments at 720 °C. Agglomerated particles are clearly seen in SEM images of samples obtained by heat-treatments at 780 °C, Fig. 5(e), and 800 °C, Fig. 5(f), at the second stage.

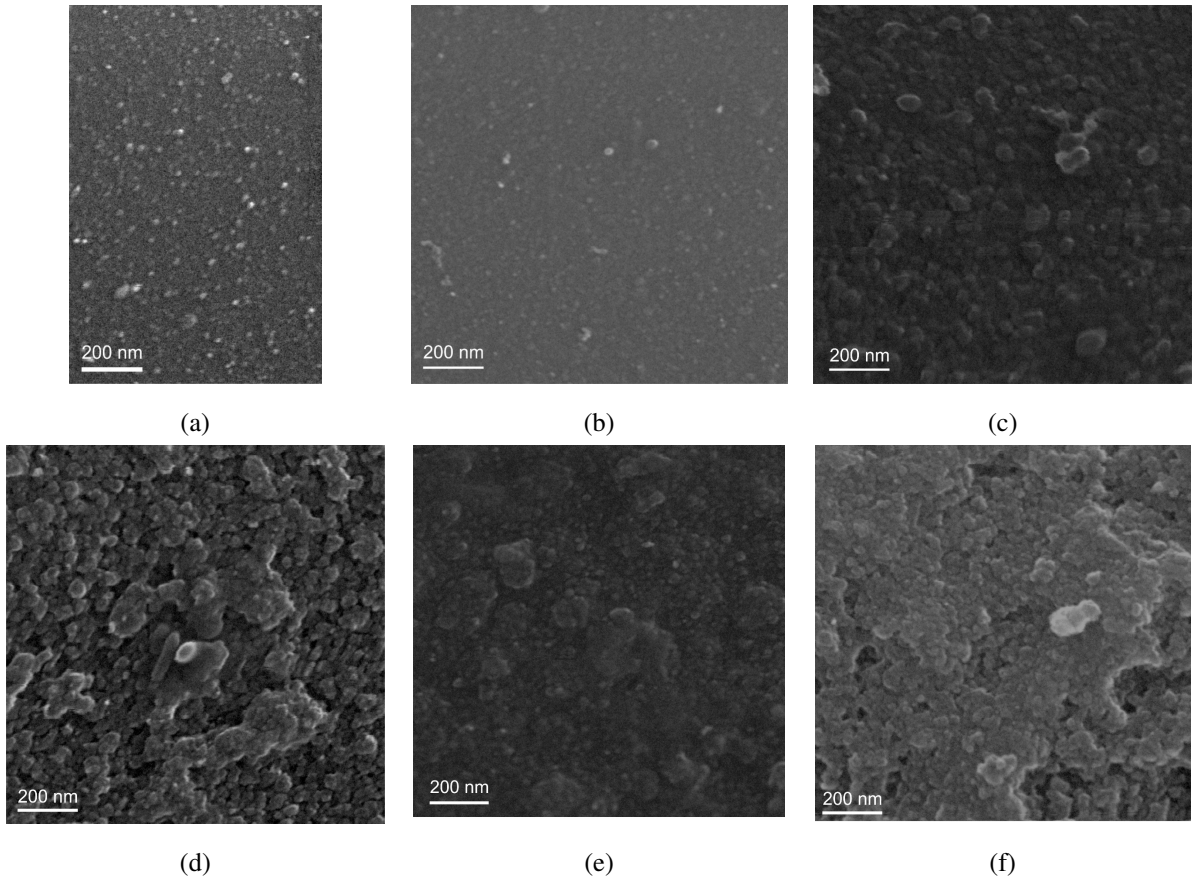

FIG. 5. SEM images of the samples under study: (a) the initial glass; (b) the glass after heat-treatment at 680 °C for 6 h; (c – f) the glasses ceramized at 680 °C for 6 h and at: (c) 720 °C for 6 h; (d) 750 °C for 6 h; (e) 780 °C for 6 h; (f) 800 °C for 6 h.

XRD patterns of glasses and glass-ceramics presented in Fig. 6(a,b) demonstrate that the initial glass and the glass heat-treated at 680 °C are X-ray amorphous. The nanocrystals with spinel structure evolve starting from the two-stage heat-treatment with a temperature at the second stage of 720 °C, while β-quartz ss and Al_2TiO_5 nanocrystals appear additionally during heat-treatments at 780 and 800 °C. The spinel lattice parameter a changes from 7.915 to 7.979 Å with an increase in the heat-treatment temperature at the second stage from 720 °C to 800 °C, while the crystal size increases more than ten times from ca. 2 to 23 nm, see Table 2. Note that according to ref. [34], the standard lattice parameter a for γ-Al_2O_3 is in the range of a = 7.900 – 7.908 Å. The lattice parameters and sizes of β-quartz ss are also presented in Table 2. The sizes increase from 29 to 39 nm with an increase of the heat-treatment temperature at the second stage from 720 to 800 °C. Table 3 shows the lattice parameters a, b, and c, and average sizes of Al_2TiO_5 crystals. The unit cell

of tieilite has three parameters. The XRD pattern of the glass-ceramic obtained by the heat-treatment at 780 °C for 6 h clearly shows only the line of Al_2TiO_5 with Miller's indices hkl (110). It is the evidence of a small fraction of Al_2TiO_5. Therefore, it is not possible to determine the lattice parameters. The lattice parameters b and c of Al_2TiO_5 crystals in the sample obtained by the heat-treatment at 780 °C for 6 h are lower than those listed in the standard ICDD card # 26-0040.

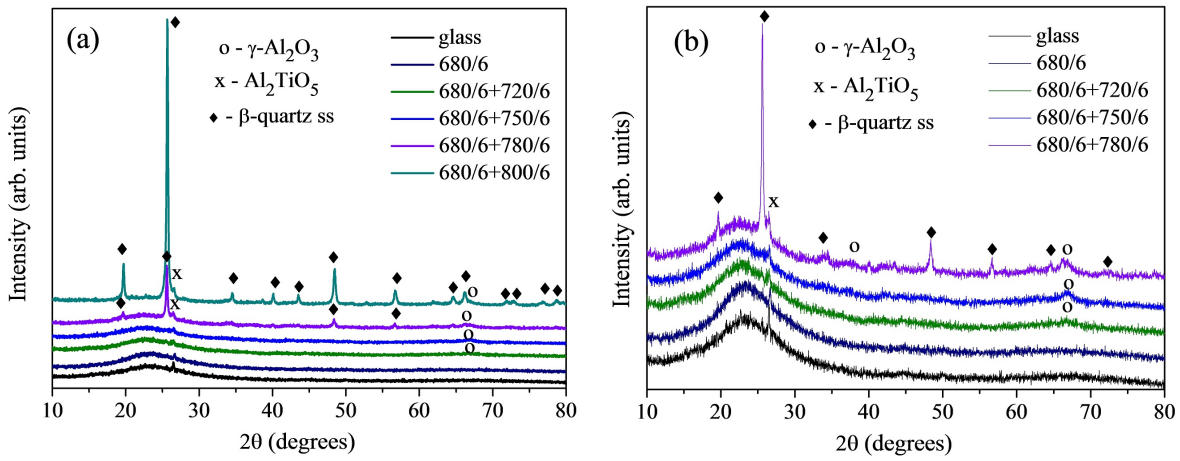

FIG. 6. XRD patterns of the initial and heat-treated glasses. Labels denote heat-treatment schedules (°C/h). The curves are shifted for the convenience of observation.

TABLE 2. Lattice parameters and average sizes of γ-Al_2O_3, and β-quartz ss crystals

Heat-treatment schedule	γ-Al_2O_3		β-quartz ss		
	a, Å	D, nm	a, Å	c, Å	D, nm
680 °C, 6 h + 720 °C, 6 h	7.915	< 2	—	—	
680 °C, 6 h + 750 °C, 6 h	7.905	5	—	—	
680 °C, 6 h + 780 °C, 6 h	7.949	8	5.220	5.439	29
680 °C, 6 h + 800 °C, 6 h	7.979	23	5.199	5.433	39

TABLE 3. Lattice parameters a, b, and c, and average sizes of Al_2TiO_5 crystals

Heat-treatment schedule	a	b	c	D, nm
680 °C, 6 h + 780 °C, 6 h	traces			20
680 °C, 6 h + 800 °C, 6 h	3.593	9.384	9.617	26

Density variation with the heat-treatment schedule presented in Fig. 7 shows that the densities of samples preliminarily heat-treated at 660 and 680 °C are only slightly higher than the density of the initial glass. The density increases rapidly when glasses are heat-treated by two-stage schedules with crystallization of dense spinel (at 720 °C and at 750 °C and then with spinel and β-quartz ss at 780 °C and at 800 °C).

Figure 8(a,b) shows absorption spectra of glasses and glass-ceramics under study. The detailed designation of absorption bands due to titanium and iron ions in different oxidation states and absorption bands assigned to interaction of these ions was performed in ref. [35] describing spectroscopy of Fe^{2+}:$MgAl_2O_4$ transparent ceramics and glass-ceramics. We will use the interpretation of absorption spectra developed in ref. [35] to explain the absorption spectra of our glasses and glass-ceramics.

The spectrum of the glass heat-treated at 680 °C for 6 h is similar to the spectrum of the initial glass, with the only exception that the position of the absorption edge shifts by about 20 nm to longer wavelengths, from 335 to 354 nm. We believe that the interaction of Fe^{3+} and Ti^{4+} ions is mainly responsible for the position of the absorption edge. The nature of the so-called ilmenite brown coloration in glasses of the LAS system nucleated solely by TiO_2 was discussed in [10] and assigned to an Fe^{3+}–O–Ti^{4+} charge transfer. The shift of the absorption edge after preliminary heat-treatment

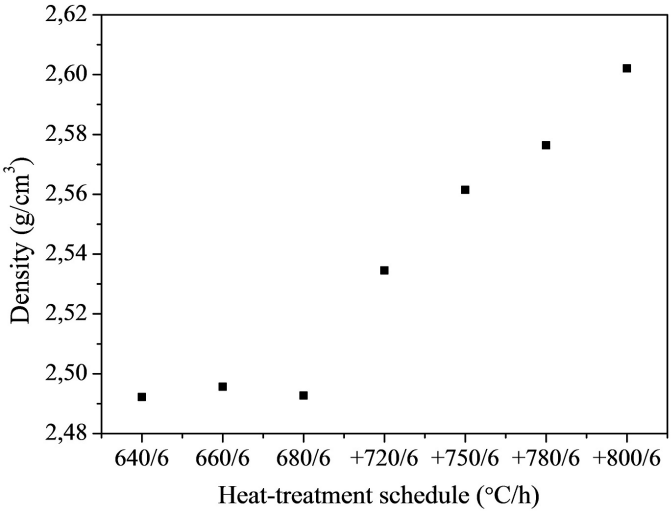

FIG. 7. Density of glasses and glass-ceramics obtained by heat-treatment schedules listed on the X-axis. The sign "+" designates the preliminary heat-treatment at 680 °C for 6 h.

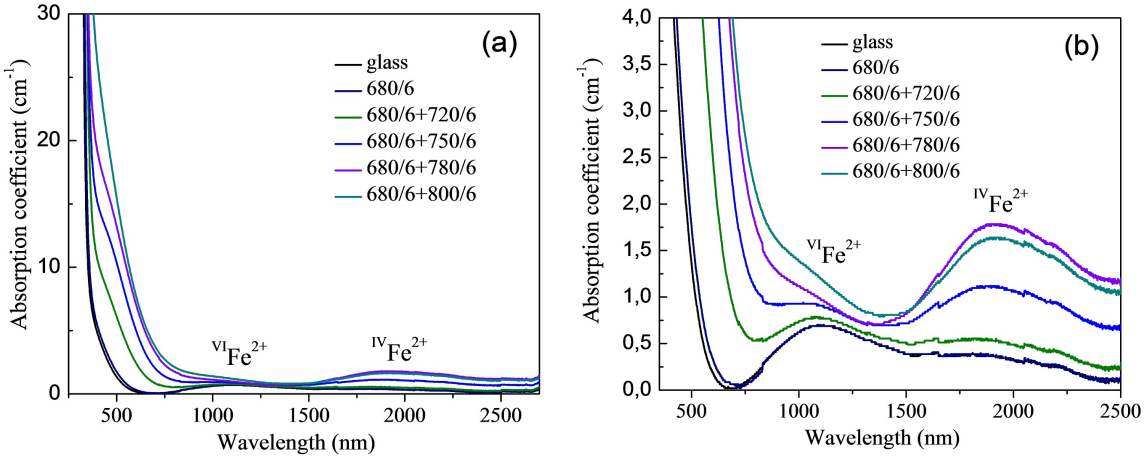

FIG. 8. (a) Absorption spectra of the initial and heat-treated glasses. (b) A closer look on spectra. Labels denote heat-treatment schedules (°C/h).

implies that Fe^{3+} ions together with titanium ions participate in the development of liquid-liquid phase separation and enter the aluminotitanate amorphous regions. The similarity of the absorption spectra of the initial glass and glass heat-treated at 680 °C testifies that Fe^{2+} ions in octahedral coordination, that are responsible for a broad absorption band with a maximum at about 1100 nm, do not participate in the development of liquid-liquid phase separation that occurs during heat-treatment at 680 °C. With an increase in the heat-treatment temperature at the second stage, there is a gradual shift of the absorption edge to longer wavelengths. In this case, absorption in the visible spectral range has multiple reasons. It is mainly caused by heterovalent charge transfer band between iron and titanium ions [10], as well as by homovalent charge transfer bands between Fe^{3+}/Fe^{2+} ions and Ti^{4+}/Ti^{3+} ions [35]. The gradual shift of this absorption edge to the visible and even near IR spectral range confirms that the iron and titanium ions participate in liquid-liquid phase separation and crystallization of the glass during two-stage heat-treatments. Raising the heat-treatment temperature at the second stage from 720 to 780 °C leads to a gradual increase in intensity of the absorption band with a maximum at ca. 1900 nm. The position of the maximum shifts from 1824 nm (the glass ceramized at 720 °C) to 1930 nm (the glass ceramized at 780 °C). The increase in the intensity of this band corresponds to the growth of the crystallinity fraction of γ-Al_2O_3. The heat-treatment at 800 °C at the second stage results in a decrease in the intensity of this absorption band, while the position of the maximum remains unchanged. Thus, based on XRD data, we may conclude that with crystallization of β-quartz ss the crystallinity fraction of γ-Al_2O_3 begins to decrease, which results in the decrease in the intensity of absorption band assigned to Fe^{2+} ions in crystals of γ-Al_2O_3. The iron ions begin to enter the structure of β-quartz ss.

4. Conclusions

The model glass and transparent glass-ceramics of the lithium aluminosilicate system nucleated by TiO_2 and doped with 0.1 % FeO were developed. The initial glass is structurally inhomogeneous yet X-ray amorphous. Fe^{2+} ions are octahedrally coordinated, which gives raise to the band with a maximum at about 1100 nm due to the $^5T_2 \rightarrow {}^5E$ (^5D) transition.

According to DSC data, the secondary heat-treatment at 660 °C for 6 h influences the glass structure but does not result in the development of three-phase immiscibility. The preliminary heat-treatment at 680 °C for 6 h significantly modifies the glass structure, which is clearly revealed in the DSC scan. It is interesting that the DSC method appears to be a powerful tool for studying the structural changes in liquid-liquid phase separated materials. It is more sensitive to structure variation than SEM, Raman, and absorption spectroscopy data for phase separated glasses of the LAS system.

Crystallization of γ-Al_2O_3 with spinel structure occurs from the phase separated amorphous regions. The average crystal sizes change from ca. 2 to 23 nm, while the lattice parameter a increases from 7.915 to 7.979 Å. Ferrous ions enter the structure of spinel crystals in tetrahedral position giving rise to a broad band absorption in the spectral range of 1930 nm due to the $^5E \rightarrow {}^5T_2$ (^5D) transition.

The precise control of the heat-treatment schedule allows tailoring the absorption properties of the developed transparent nanophase glass-ceramics.

References

[1] Method of Making Ceramics and Product Thereof. Method of Making Ceramics and Product Thereof: patent 2920971 U.S. Stookey, S.D. January 12, 1960.

[2] Bach H., Krause D. *Low Thermal Expansion Glass Ceramics*, Springer-Verlag Berlin Heidelberg, 2005, 246 p.

[3] Höland W., Beall G.H. *Glass-Ceramic Technology*, Wiley: Hoboken, NJ, USA, 2012, 414 p.

[4] Zanotto E.D. A bright future for glass-ceramic. *Am Ceram Soc Bull.,* 2010, **89** (8), P. 19–27.

[5] Venkateswaran C., Sreemoolanadhan H., Vaish R. Lithium aluminosilicate (LAS) glass-ceramics: a review of recent progress. *Int. Mater. Rev.,* 2022, **67** (6), P. 620–657.

[6] Zandona A., Patzig C., Rüdinger B., Hochrein O., Deubener J. TiO_2(B) nanocrystals in Ti-doped lithium aluminosilicate glasses. *J. Non-Cryst. Solids*, 2019, **2**, 100025.

[7] Fernandez-Martin C., Bruno G., Crochet A., Ovono D.O., Comte M., Hennet L. Nucleation and growth of nanocrystals in glass-ceramics: an in situ SANS perspective. *J. Am. Ceram. Soc.,* 2012, **95** (4), P. 1304–1312.

[8] Glatz P., Comte M., Montagne L., Doumert B., Cousin F., Cormier L. Structural evolution at short and medium range distances during crystallization of a P_2O_5–Li_2O–Al_2O_3–SiO_2 glass. *J. Am. Ceram. Soc.,* 2020, **103** (9), P. 4969–4982.

[9] Vigier M., Deniard P., Gautron E., Gautier N., Genevois C., Ory S., Allix M., Kacem I.B., Jobic S. Microstructural insights on lithium aluminum silicate (LAS) glass ceramics. *Ceram. Int.*, 2024, **50** (16), P. 29011–29015.

[10] Kleebusch E., Patzig C., Krause M., Hu Y., Höche T., Rüssel C. The effect of TiO_2 on nucleation and crystallization of a Li_2O–Al_2O_3–SiO_2 glass investigated by XANES and STEM. *Sci. Rep.,* 2018, **8**, 2929.

[11] Kleebusch E., Patzig C., Höche T., Rüssel C. The evidence of phase separation droplets in the crystallization process of a Li_2O–Al_2O_3–SiO_2 glass with TiO_2 as nucleating agent – An X-ray diffraction and (S)TEM-study supported by EDX-analysis. *Ceram. Int*., 2018, **44**, P. 2919–2926.

[12] Naumov A.S., Shakhgildyan G.Y., Golubev N.V., Lipatiev A.S., Fedotov S.S., Alekseev R.O., Ingat'eva E.S., Savinkov V.I., Sigaev V.N. Tuning the coefficient of thermal expansion of transparent lithium aluminosilicate glass-ceramics by a two-stage heat treatment. *Ceram.,* 2023, **7** (1), P. 1–14.

[13] Raghuwanshi V.S., Rüssel C., Hoell A., Crystallization of $ZrTiO_4$ nanocrystals in lithium-alumino-silicate glass ceramics: anomalous small-angle X-ray scattering investigation. *Cryst. Growth Des.,* 2014, **14** (6), P. 2838–2845.

[14] Höche T., Patzig C., Gemming T., Wurth R., Rüssel C, Avramov I., Temporal evolution of diffusion barriers surrounding $ZrTiO_4$ nuclei in lithia aluminosilicate glass-ceramics. *Cryst. Growth Des*., 2012, **12** (3), P. 1556–1563.

[15] Zheng T., Li M.H., Ma Y.P., Jiang H. Kinetic analysis of the crystallization of Y_2O_3 and La_2O_3 doped Li_2O–Al_2O_3–SiO_2 glass. *RSC Adv*., **14** (10), P. 7052–7060.

[16] Li B., Wang S., Fang Y. Effect of Cr_2O_3 addition on crystallization, microstructure and properties of Li_2O–Al_2O_3–SiO_2 glass-ceramics. *J. Alloys Compd*., 2017, **693**, P. 9–15.

[17] Lilensten L., Fu Q., Wheaton B.R., Credle A.J., Stewart R.L., Kohli J.T. Kinetic study on lithium-aluminosilicate (LAS) glass-ceramics containing MgO and ZnO. *Ceram Int*., 2014, **40** (8 PART A), P. 11657–11661.

[18] Alekseeva I.P., Dymshits O.S., Tsenter, M.Y., Zhilin A.A. Influence of various alkali and divalent metal oxides on phase transformations in NiO-doped glasses of the Li_2O–Al_2O_3–SiO_2–TiO_2 system. *J. Non-Cryst. Solids*, 2011, **357**, P. 2209-2214.

[19] Dymshits O., Bachina A., Alekseeva I., Golubkov V., Tsenter M., Zapalova S., Bogdanov K., Danilovich D., Zhilin A. Phase transformations upon formation of transparent lithium alumosilicate glass-ceramics nucleated by yttrium niobates. *Ceram*., 2023, **6**, P. 1490–1507.

[20] Sun T., Zheng C., Zhang F., Zhang J., Han J., Xie J., He J., Jiang H. Mixed CaO/MgO effect on microstructure, mechanical properties and crystallization behaviour of Li_2O–Al_2O_3–SiO_2–ZrO_2–P_2O_5 glass. *J. Non-Cryst. Solids*, 2023, **616**, 122457.

[21] Guo Y., Wang J., Ruan J., Han J., Xie J., Liu C. Microstructure and ion-exchange properties of glass-ceramics containing $ZnAl_2O_4$ and β-quartz solid solution nanocrystals, *J. Eur. Ceram. Soc*., 2021, **41** (10), P. 5331–5340.

[22] Rao C.S., Rao M.C., Srikumar T. Optical absorption studies on lithium aluminosilicate glasses doped with low concentrations of WO_3. *Int. J. Chemtech Res*., 2014, **6** (7), P. 3935–3938.

[23] Dymshits O., Shepilov M., Zhilin A. Transparent glass-ceramics for optical applications. *MRS Bull*., 2017, **42**, P. 200–205.

[24] Dymshits O.S., Alekseeva I.P., Zhilin A.A., Tsenter M.Y., Loiko P.A., Skoptsov N.A., Malyarevich A.M., Yumashev K.V., Mateos X., Baranov A.V. Structural characteristics and spectral properties of novel transparent lithium aluminosilicate glass-ceramics containing (Er,Yb)NbO_4 nanocrystals. *J. Lumin.,* 2015, **160**, P. 337–345.

[25] Loiko P.A., Dymshits O.S., Alekseeva I.P., Zhilin A.A., Tsenter M.Y., Vilejshikova E.V., Yumashev K.V., Bogdanov K.V. Structure and spectroscopic properties of transparent glass-ceramics with (Eu^{3+},Yb^{3+}):$YNbO_4$ nanocrystals. *J. Lumin.,* **2016**, **179**, P. 64–73.

[26] Alekseeva I.P., Bobovich Y.S., Tsenter M.Y., Chuvaeva T.I. Raman spectra of glass ceramics belonging to the Li_2O–Al_2O_3–SiO_2–TiO_2 system and the nature of the phases containing titanium. *J. Appl. Spectrosc*., 1981, **35**, P. 1008–1012.
[27] Schneider C.A., Rasband W.S., Eliceiri K.W. NIH Image to ImageJ: 25 years of image analysis. *Nat. Methods*, 2012, **9** (7), P. 671–675.
[28] Lipson H., Steeple H., in: McMillan (Ed.), Interpretation of X-Ray Powder Patterns, Martins Press, London, N.Y., 1970, p. 344.
[29] Ovono Ovono D., Berre S., Pradeau P., Comte M., Bruno G., Study of the crystallization kinetics of LAS glass by differential scanning calorimetry, X-ray diffraction, and beam bending viscometry. *Thermochim. Acta*, 2012, **527**, P. 158–164.
[30] Dymshits O.S., Zhilin A.A., Petrov V.I., Tsenter M.Ya., Chuvaeva T.I., Golubkov V.V. A Raman spectroscopic study of phase transformations in titanium-containing lithium aluminosilicate glasses. *Glass Phys. Chem*., 1998, **24**, P. 79–96.
[31] Eremeev K., Dymshits O., Alekseeva I., Khubetsov A., Zapalova S., Tsenter M., Basyrova L., Serres J.M., Mateos X., Loiko P., Popkov V., Zhilin A. Effect of redox conditions of glass melting on the structure and the properties of titanium-containing gahnite glass-ceramics. *J. Eur. Ceram. Soc*., 2024, **44**, P. 3362–3380.
[32] Alekseeva I.P., Belyaevskaya N.M., Bobovich Ya.S., Tsenter M.Ya., Chuvaeva T.I. Recording, interpretation, and some examples of application of Raman spectra for glass ceramics activate with titanium (IV) oxide. *Opt. Spectrosc*., 1978, **45**, P. 927–936.
[33] Sprengard R., Binder K., Brandle M., Fotheringham U., Sauer J., Pannhorst W. On the interpretation of the experimental Raman spectrum of β-eucryptite $LiAlSiO_4$ from atomistic computer modeling. *J. Non-Cryst. Solids*, 2000, **274**, P. 264–270.
[34] Shirasuka K., Yanagida H., Yamaguchi G. The preparation of η-alumina and its structure. *Mater. Sci.*, 1976, **84**, P. 610–613.
[35] Basyrova L., Bukina V., Balabanov S., Belyaev A., Drobotenko V., Dymshits O., Alekseeva I., Tsenter M., Zapalova S., Khubetsov A., Zhilin A., Volokitina A., Vitkin V., Mateos X., Serres J.M., Camy P., Loiko P. Synthesis, structure and spectroscopy of Fe^{2+}:$MgAl_2O_4$ transparent ceramics and glass-ceramics. *J. Lumin*., 2021, **236**, 118090.

Accepted 7 December 2024

Information about the authors:

Kristina A. Trukhanova – Nordwestlab LLC, 15.2 Line 26th of Vasilyevsky Island, St. Petersburg, 199106, Russia; ORCID 0000-0001-5587-4037; kristina.truhanova@gmail.com

Olga S. Dymshits – Ioffe Institute, 26 Politekhnicheskaya, St. Petersburg, 194021, Russia; Vavilov State Optical Institute, 36 Babushkina, St. Petersburg, 192171, Russia; ORCID 0000-0003-1980-0561; vodym1959@gmail.com

Irina P. Alekseeva – Vavilov State Optical Institute, 36 Babushkina, St. Petersburg, 192171, Russia; vgolub19@gmail.com

Kirill V. Bogdanov – Saint Petersburg National Research University of Information Technologies, Mechanics and Optics, Kronverkskiy, 49, St. Petersburg, 197101, Russia; ORCID 0000-0003-4243-1354; kirw.bog@gmail.com

Svetlana S. Zapalova – Vavilov State Optical Institute, 36 Babushkina, St. Petersburg, 192171, Russia; zenii99@yandex.ru

Maksim I. Tenevich – Ioffe Institute, 26 Politekhnicheskaya, St. Petersburg, 194021, Russia; ORCID 0000-0003-2003-0672; mtenevich@gmail.com

Anastasia K. Bachina – Ioffe Institute, 26 Politekhnicheskaya, St. Petersburg, 194021, Russia; ORCID 0000-0001-7015-1435; a.k.bachina@yandex.ru

Vadim I. Popkov – Ioffe Institute, 26 Politekhnicheskaya, St. Petersburg, 194021, Russia; ORCID 0000-0002-8450-4278; vip-07@yandex.ru

Aleksandr A. Zhilin – D. V. Efremov Institute of Electrophysical Apparatus, 3 Doroga na Metallostroi, pos. Metallostroi, St. Petersburg, 196641, Russia; ORCID 0000-0002-6681-6577; zhilin1311@yandex.ru

Conflict of interest: the authors declare no conflict of interest.